Research Paper

Centrifuge Modeling of the Monotonic Capacity of Offshore Ring Anchors in Sand

Huang, L.[1]*, Martinez, A.[2]*, Aubeny, C.[3], DeGroot, D.[4], Arwade, S.[5] and Beemer, R.[6]

Abstract: The development of offshore wind technology has become a feasible solution to meet the increasing demands for clean and renewable energy. The United States has a total of 4250GW offshore wind energy potential; however, 65% of it is in deep water zones (Lopez *et al.*, 2022) where wind turbines with fixed foundations typically are economically and technically unfeasible. In those situations, floating turbines supported by subsea anchors are a more competitive solution. Based on previous studies, ring anchors can be more material-efficient than piles and caissons because they require less material. Ring anchors also perform better than drag anchors due to their greater embedment depth. To further understand the behavior of ring anchors in saturated sand, a series of centrifuge load tests were performed at the University of California Davis Center for Geotechnical Modeling (CGM) at an acceleration of 70g. This test series investigated the effect of the anchor embedment depth and loading angle on the monotonic loading behavior. The ring anchor models were embedded in dense saturated sand, and then connected to an actuator using taut steel wire ropes. Sensors were used to measure the line tension, displacement, and inclination. The results indicate that the ring anchors mobilize greater capacities as their embedment depth is increased and when they are loaded at angles close to the horizontal direction, while vertical loading leads to the smallest capacity. The anchor displacement during the tests deviated slightly from the loading direction, showing a horizontal deviation at the earlier stages of the tests and a vertical one after the peak load. Furthermore, soil disturbance induced by the anchor installation was found to have a strong effect on the vertical capacity of the ring anchors. Overall, this study provides valuable information regarding the monotonic loading behavior of ring anchors which can aid in their future field deployment.

Keywords: floating offshore, ring-shaped anchor, offshore anchor, centrifuge modeling

Introduction

Offshore Floating Wind Farm

In recent years, the development of offshore wind farms has become a trending solution to meet the growing demand for clean and renewable energy. Along the east coast of the United States, several offshore wind farms have been operational for several years, with more under planning. On the west coast, two potential locations for wind farms have been identified by the Bureau of Ocean Energy Management (BOEM), and the lease was finalized in December 2022 (BOEM, 2023). Constructing an offshore wind farm on the west coast poses unique challenges, primarily due to its substantial water depth. In fact, 65% of United States offshore wind resources are located in deep water regions, where water depth is greater than 60m (Lopez *et al.*, 2022). In such cases, the use of fixed foundations for offshore wind turbines becomes economically and technically impractical due to the large amounts of material needed and the high load magnitudes. Instead, floating platforms with a mooring system and subsea anchors present a more feasible solution (Musial *et al.*, 2018). While floating platforms with mooring systems may satisfy the technical requirements, their high costs can become a significant obstacle to the development of deep-water wind farms, as evidenced by the cancellation of the Atlantic Array wind farm project (Bhattacharya 2014; Carter 2007). For floating wind turbines, the foundation system typically accounts for 25% to 35% of the total construction cost (Lee *et al.*, 2020). Therefore, optimizing the design of the foundation system becomes cru-

[1] Ph.D. student, University of California Davis, 2001 Ghausi Hall, Davis, CA 95616, USA
[2] Associate professor, University of California Davis, 3103 Ghausi Hall, Davis, CA 95616, USA
[3] Professor, Texas A&M University, DELB 808P 201 Dwight Look Engineering Bldg., College Station, TX 77843, USA
[4] Professor, University of Massachusetts Amherst, Marston Hall Room 20, 130 Natural Resources Road, Amherst, MA 01003, USA
[5] Professor, University of Massachusetts Amherst, Marston Hall Room 223, 130 Natural Resources Road, Amherst, MA 01003, USA
[6] Assistant Professor, University of Massachusetts Dartmouth, Violette Research 220A, North Dartmouth, MA 02747, USA
* Corresponding author email: hlhuang@ucdavis.edu (or amart@ucdavis.edu)

Print ISSN: 1937-5247 Online ISSN: 1937-5255
Published by Deep Foundations Institute
Received 15 September 2023; received in revised form 24 April 2024; accepted 25 April 2024
https://doi.org/10.37308/DFIJnl.20230915.297

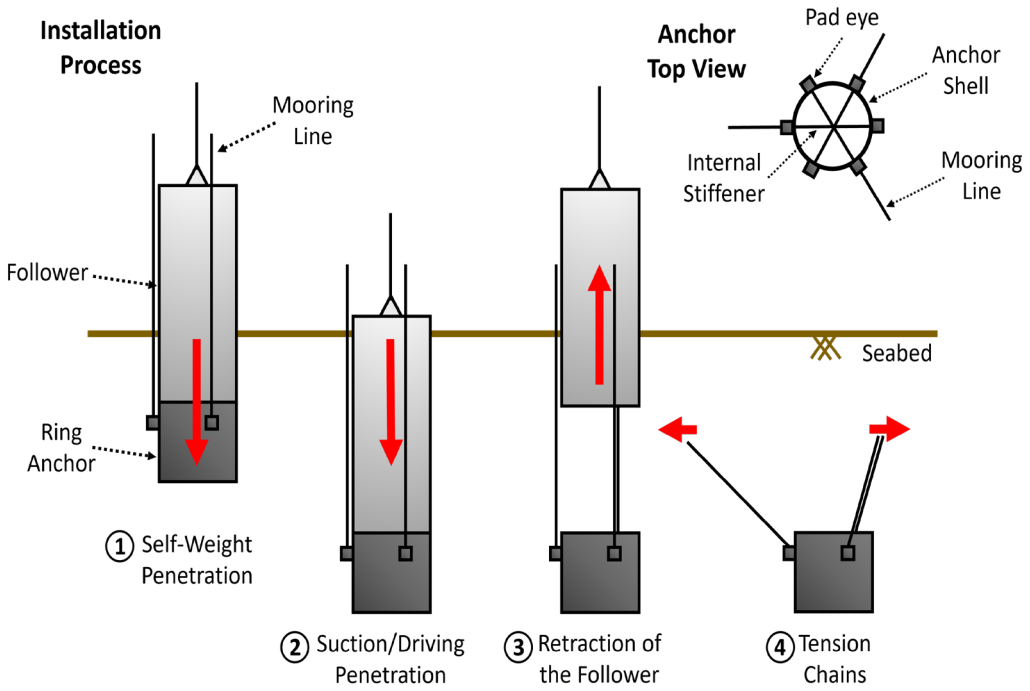

Figure 1. Ring anchor and proposed installation procedure

cial to reducing the capital cost of deep-water offshore wind farms. This optimization process can encompass various aspects, such as reducing transportation and installation costs, maximizing the geotechnical efficiency of the anchors, and minimizing the overall number of anchors required for a wind farm, among others.

Ring Anchor

The capacity of subsea anchors is directly related to the strength of the soil; thus, deep embedment is important for their performance. Furthermore, considering the complex geology of offshore environments, subsea anchors are required to be deployable in different soil conditions, such as soft or stiff clay, sand, and layered profiles. While most anchor types can be embedded deeply in soft clay deposits, only a few of them can achieve deep embedment in stiff clay or sand (Diaz, 2016), resulting in limited capacity that can lead to excessive deformation or anchor pullout.

In current practice, offshore floating platforms are usually anchored to the seabed using piles or suction caisson. Drag anchors are also being used in some of the projects, but primarily for sites with soft clay (Aubeny, 2017). In recent years, the new ring anchor has been proposed as another viable solution. Figure 1 illustrates the concept of the ring anchor and the proposed installation method. Based on previous studies, ring anchors can be more efficient than driven piles and caissons because they require less material and less transportation effort. Also, ring anchors perform better than drag anchors due to their greater embedment depth and the fact that they can be deployed in different soil types (Lee and Aubeny, 2020). In addition, the multiline potential of the ring anchor is another significant advantage. Enabling the connection of multiple floating wind turbines to a single anchor allows a reduction in the total number of anchors required. This reduction leads to cost savings in various aspects, including site characterization, manufacturing, transportation, and installation (Fontana, 2019).

This paper investigates the behavior of ring anchors embedded in saturated sand under monotonic tensile loading. This study uses centrifuge modeling to investigate the effect of the embedment depth and loading direction on the load-displacement behavior and capacity of the ring anchors. These tests are part of a larger project focused on evaluating the monotonic and cyclic performance of ring anchors in both sandy and clayey soils in both single-line and multi-line configurations.

Materials and Methods

Centrifuge Modeling

To further understand the behavior of ring anchors in saturated sand, a series of centrifuge monotonic tensile load tests were performed at the University of California Davis Center for Geotechnical Modeling (CGM) using the 9-meter-radius centrifuge. The method of centrifuge modeling has been proven to be an effective method to study the behavior of various offshore anchors (Beemer, 2016; Herduin, 2019; Zhao *et al.*, 2020). As the centrifuge spins at an angular velocity, it creates a centrifugal acceleration that allows performing tests on scaled models. This allowed matching the stress magnitude and distribution of the field-scale structure (*i.e.*, prototype) in a reduced-scale model (*i.e.*, model). For this test series, an acceleration of 70 times Earth's gravity

Table 1. Centrifuge scaling laws

Quantity	Symbol	Equation
Length/depth	L	$\frac{L_P}{L_M} = N$
Force	F	$\frac{F_P}{F_M} = N^2$
Stress/pressure	σ	$\frac{\sigma_P}{\sigma_M} = 1$

The subscripts $_P$ and $_M$ stand for prototype and model scales.

(*i.e.*, 70 g) was used. The centrifuge scaling laws between the experimental prototype and model are related to the ratio of applied acceleration to Earth's gravity (N) (Garnier *et al.*, 2007). Scaling laws that are relevant to this centrifuge test are presented in Table 1. More centrifuge scaling law information can be found in Kutter *et al.* (2019). All the quantities provided throughout this paper are in prototype scale, unless otherwise noted.

Saturated Sand Deposit

In this study, all tests were conducted in saturated sand deposits constructed with Ottawa F-65 sand, which is a poorly-graded fine silica sand. The sand has a median particle size, D_{50}, of 0.23mm, minimum void ratio, e_{min}, of 0.48, maximum void ratio, e_{max}, of 0.78, and peak and residual friction angles of 33.8° and 29.6° (Bastidas, 2016; Martinez *et al.,* 2019). The Ottawa F-65 sand has similar properties as offshore sands reported in the literature, including medium-dense and dense fine sands with median particle size around 0.20 mm and in many instances no fines content (Jardine *et al*. 1998; Jensen and Kellezi 2023). The soil specimens were prepared by air pluviating sand into the model container in lifts with a thickness of 25mm. The rectangular container utilized for the experiments has internal prototype dimensions of 115.5m in length, 55.3m in width, and 42.0m in depth (1.65m, 0.79m, and 0.6m, respectively, in model scale). The sand deposits have a depth of 31.5m (0.45m in model scale). Two models were built to perform the load tests, with relative densities of 78.8% and 79.2% determined from mass and volume measurements. The first model was saturated using the top-down method, while the second model was saturated using the bottom-up method through a pre-embedded gravel layer and

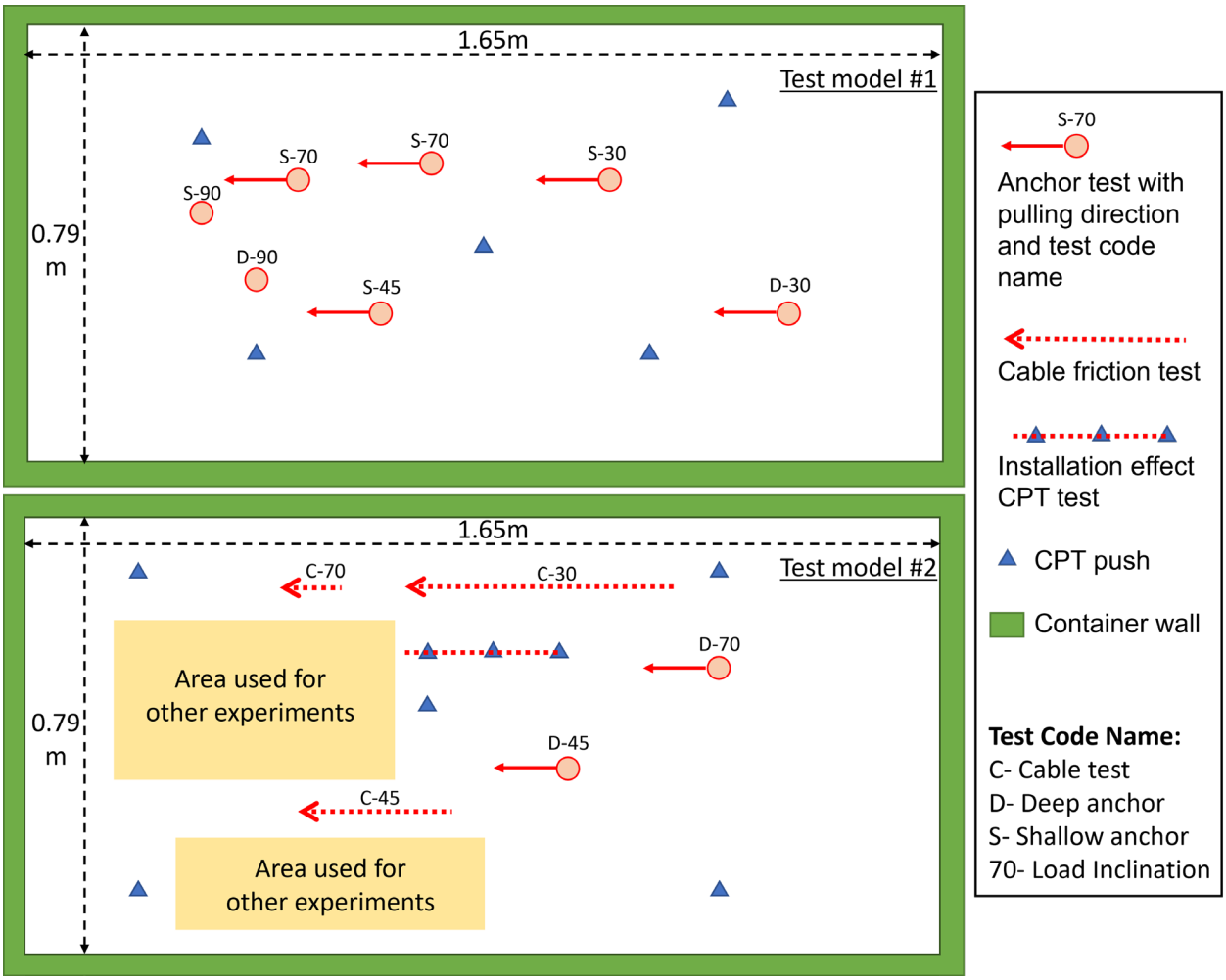

Figure 2. Top view of the test layout for the centrifuge test model #1 and #2 (dimensions in model scale)

a vertical well. Figure 2 shows a 2D test layout for the sand models used in this study.

Ring Anchor Model

The ring anchor model used for the centrifuge tests has a diameter (D) of 2.8m (40mm in model scale), length (L) of 4.2m (60mm in model scale), and wall thickness (t) of 0.14 m (2 mm in model scale). The ring anchors were 3D printed using 17-4 high-strength stainless steel. The anchors were installed at embedment depths equivalent to 3D and 6D, corresponding to depths of 8.4m and 16.8m, measuring from the top of the anchor to the soil surface. For the deeply embedded anchors, there is a distance of 10.5m between the bottom of the anchor and the container's base. Actuators were used to load the ring anchors via taut stainless-steel ropes. The connection between the steel rope and the anchor consists of a swaged ball that rests on a depression in the side wall of the anchor. When a tensile load is applied, the swaged ball is pulled against the anchor wall, causing stress concentration around the through-hole connection. To mitigate this, stiffeners were added inside the anchor to avoid permanent deformations of the connection points.

Testing Plan

A total of eight anchor tensile load tests were conducted, encompassing two different embedment depths and four load inclination angles. In the shallow embedment case, the anchor was positioned at a depth of 8.4m (3D), resulting in an effective stress of 109kPa at the anchor's mid-height. For the deep embedment case, the anchor was embedded at a depth of 16.8m (6D), resulting in an effective stress of 196kPa at the anchor's mid-height. Tests were performed at four load inclination angles by adjusting the wire rope-anchor attachment and load application angles. Tests were performed at 30°, 45, 70°, and 90° (vertical) load inclination angles measured from the horizontal direction. Each test involved an anchor displacement equivalent to 1.5 D (4.2m, or 60mm in model scale) to capture the anchor's behavior in both pre-peak and post-peak stages.

Loading System

During the experiments, a tensile load was applied to the embedded anchors through the steel wire ropes using a linear actuator. The wire rope was connected to the actuator using a swaged loop and fork-pin connection. A photograph showing the different elements of the loading system is presented in Figure 3. The actuator is specially designed to accommodate operating under 70g conditions. Specifically, two steel rods were added to reduce the actuator's deflection due to self-weight. The actuator has a total stroke length of 76.2 mm in model scale, with a model scale tensile capacity of 7.56kN. A servo motor was used to drive the actuator through a 20:1 gearbox and a 2:1 belt transmission. Extra aluminum pieces were added between the motor and actuator as reinforcement for increasing stiffness to prevent sagging. The actuator was assembled with an aluminum bracket with angle adjustment features. By rotating the outer plate and inserting a screw in different holes, the actuator can be set to form a 30°, 45°, 70°, and 90° angle with the outer plate for loading the anchors in different inclinations (Figure 3 shows loading at 70°). During experiments, the whole actuator system was supported by an aluminum cross beam.

Sensors

An 8.9kN load cell and a linear potentiometer with a stroke of 76.2mm were attached to the actuator to track the tensile force and displacement of the wire rope, respectively. To

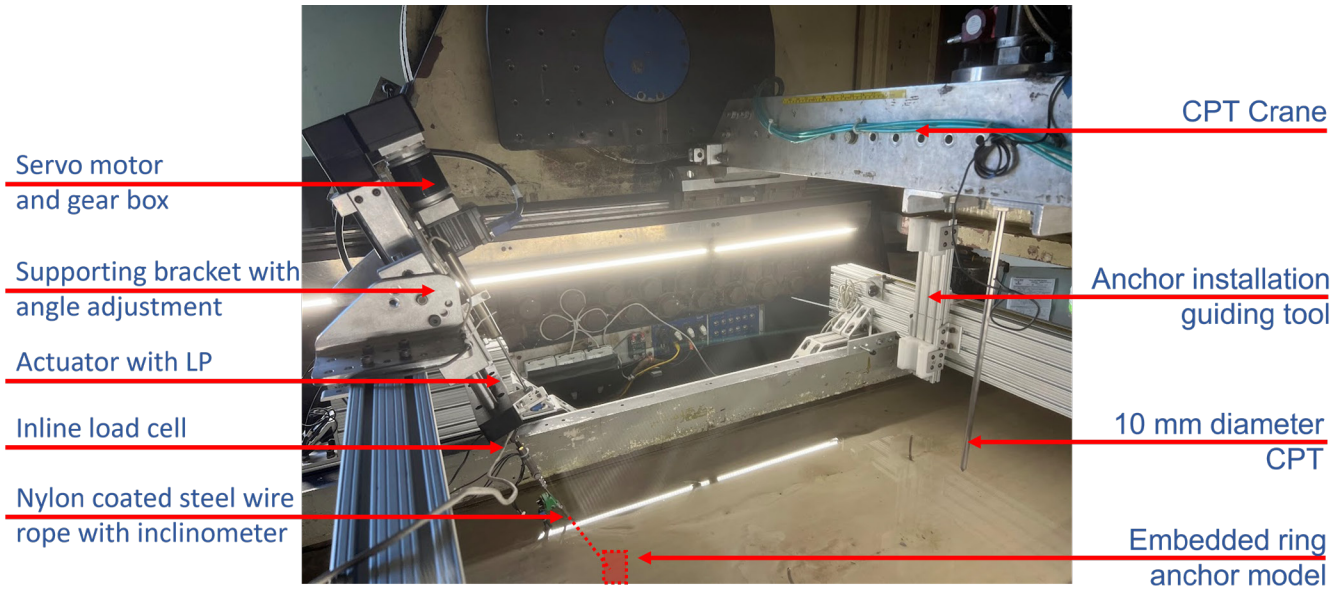

Figure 3. Complete anchor tensile load test apparatus with the anchor embedded in sand model

measure the change in inclination angle of the wire rope, an inclinometer made with a 3-axis 10G MEMS accelerometer (Beemer *et al.*, 2018) was suspended on the wire rope during the tests. Three cameras were mounted at various locations to capture videos of the pulling process from different angles. Two pairs of bender elements were embedded at different depths within the sand model to measure the shear wave velocity. Moreover, two pore water pressure transducers were embedded at the bottom of the soil model to monitor the location of the water table.

Anchor Installation Method

All the anchors were installed by quasi-static pushing at 1g conditions. An installation tool was designed and built for installing the anchors at the desired depth and location, as shown in Figure 4. This tool features a pusher tube with a slightly larger outer diameter than the anchors, along with six securely welded pins at its base to prevent any horizontal movement of the anchor. The anchors were pushed by slowly lowering a large mass on top of the installation tool. A triangle wing with welded pins ensures that the wire ropes are installed at the desired angle of loading (*i.e.*, 30°, 45, 70°, and 90°). A pusher guide allows to maintain verticality and avoid anchor tilting during installation. After installation is completed, the installation tool is slowly lifted, leaving the ring anchor and wire rope embedded in the soil.

Repeateability and Correction for Wire Rope Stretching, Friction, and Slack

The repeatability of the test results was addressed by performing the shallow test at 70 degrees twice. The results indicate a high similarity in the load-displacement curve, with a difference in measured peak capacity of less than 5%. To examine the potential error in displacement measurement resulting from elongation of the wire rope, a series of elongation tests were conducted. The experimental setup involved pulling on one end of a wire rope with its opposite end attached to a stiff frame, while the wire rope tension and displacement are measured. To ensure accurate results and to separate the elongation effect for the wire rope and the connection points (*i.e.*, shank ball swage end and loop swage end), five wire ropes of different lengths were tested. The test outcomes revealed that the elongation effect was minimal, and a correction method based on wire rope length was developed. Specially, the elongation coefficient of the wire rope was 1% for every 4.58kN of model scale force, while the elongation coefficient of the connection was 1% for every 5.09kN.

A series of centrifuge wire rope-only tensile loading tests were conducted to examine the frictional force between the wire rope and the soil. In these tests performed at 70g, wire ropes were embedded in sand and pulled. As shown in Figure 5a, the test results revealed that, in the case of deep embedment, the peak frictional force is around 0.5 MN. The residual frictional force exerted on the wire rope ranged between 0.17 to 0.25 MN, which is approximately 1% to 3% of the total tensile force measured during anchor pullout tests. This indicates that the contribution of the wire rope-soil friction can be neglected when estimating anchor capacities.

Slack of the wire rope impacted the load-displacement results at the early stages of the tests. As the tensile force increases, it initially straightens the wire rope before actually loading the anchor, resulting in an initial soft response. Consequently, the recorded displacement of the actuator was adjusted as shown in Figure 5b. Specifically, the steep increase in load characteristic of the initial loading response was extrapolated to a displacement of 0m.

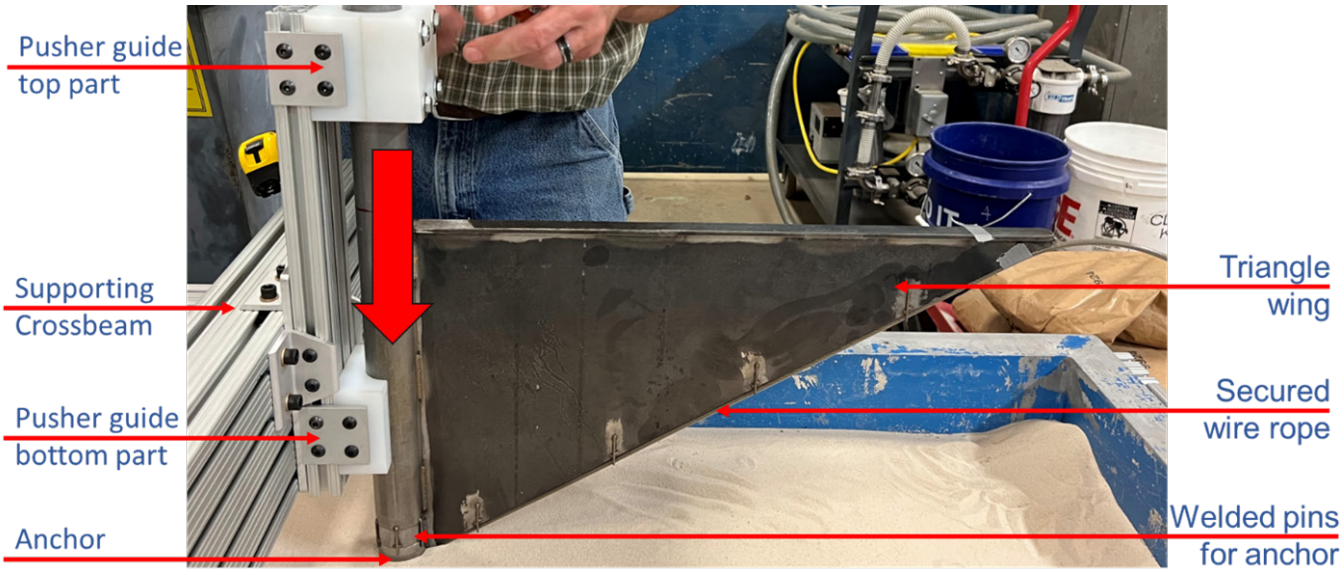

Figure 4. Anchor installation tool for pushing anchor in at 1g condition

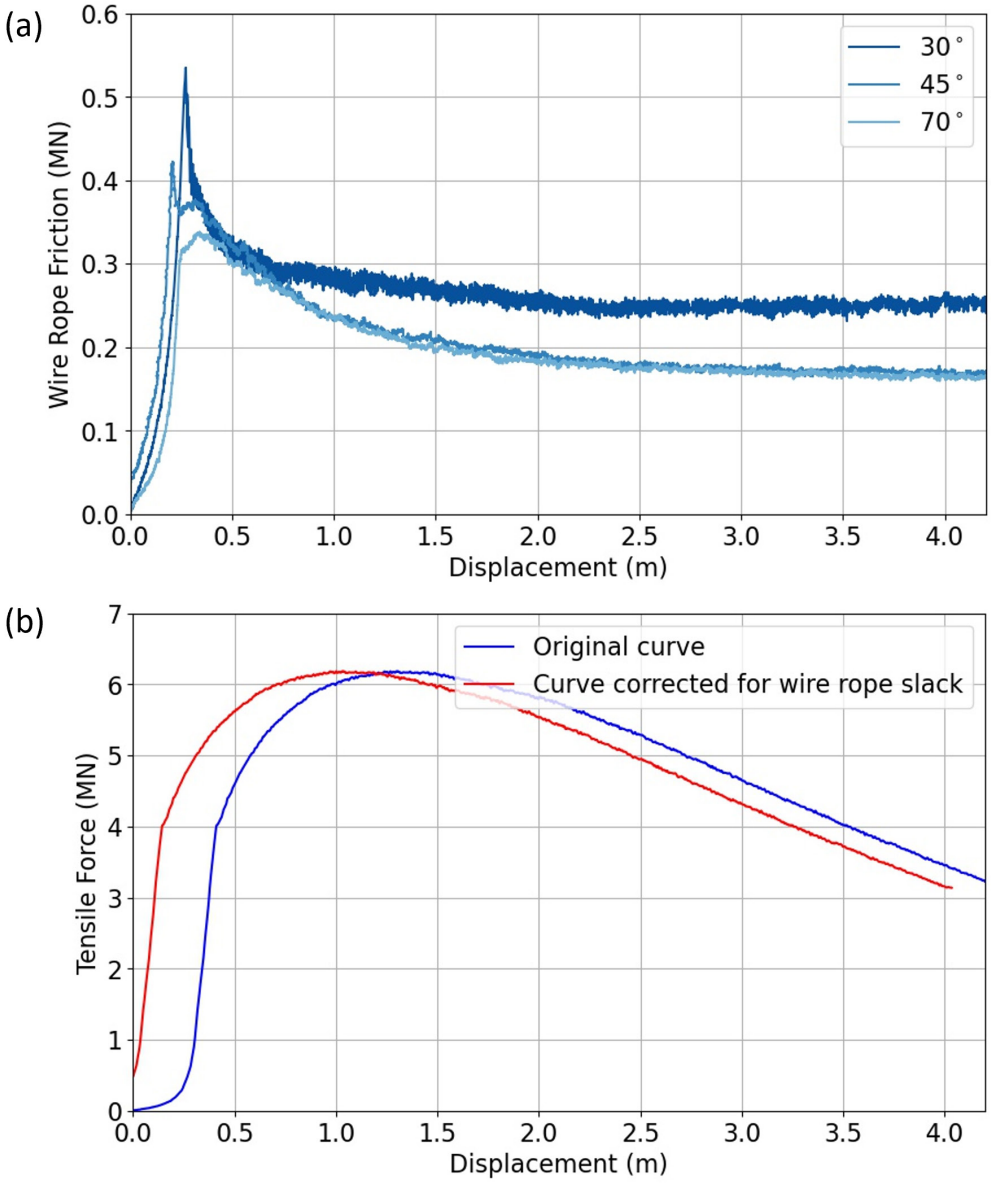

Figure 5. (a) Deeply embedded wire rope friction for different inclination angles and (b) Correcting the force-displacement curve for wire rope slack

Results

Cone Penetration Test (CPT) Results

To examine the relative density and uniformity of the soil deposits, several in-flight CPT soundings were performed at different locations of the model using a 10 mm diameter CPT probe. Results are shown in Figure 6. The traces of CPT tip resistance (q_c) indicate an increase with depth, as shown in Figure 6a. The q_c values were used to estimate relative density (D_R) distributions with depth using the Mayne (2007) correlation, as shown in Figure 6b. The D_R data at depths smaller than 11m is not presented because it is impacted by shallow penetration effects, as described in detail by Kim *et al.* (2016), which results in an underestimation of the soil relative density using the empirical correlation. The CPT result shows a slight increase in D_R with depth and little lateral spatial variability. The average D_R is about 79%, which agrees with the sand pluviation records using mass and volume indicating an average D_R of 78.8% and 79.2% for the first and second soil models, respectively. In addition, Figure 6c plots the shear wave velocity (V_S) obtained from the bender elements data against the corresponding vertical effective stress. To obtain data at different effective stresses, measurements were taken at g-levels of 20g, 40g, 60g, and 70g. Figure 6c shows that for both soil models, the V_S increases as the effective stress increases following a power function trend as described in Cha *et al.* (2014). The q_c and V_S results indicate that the relative density of both models is uniform and close to one another.

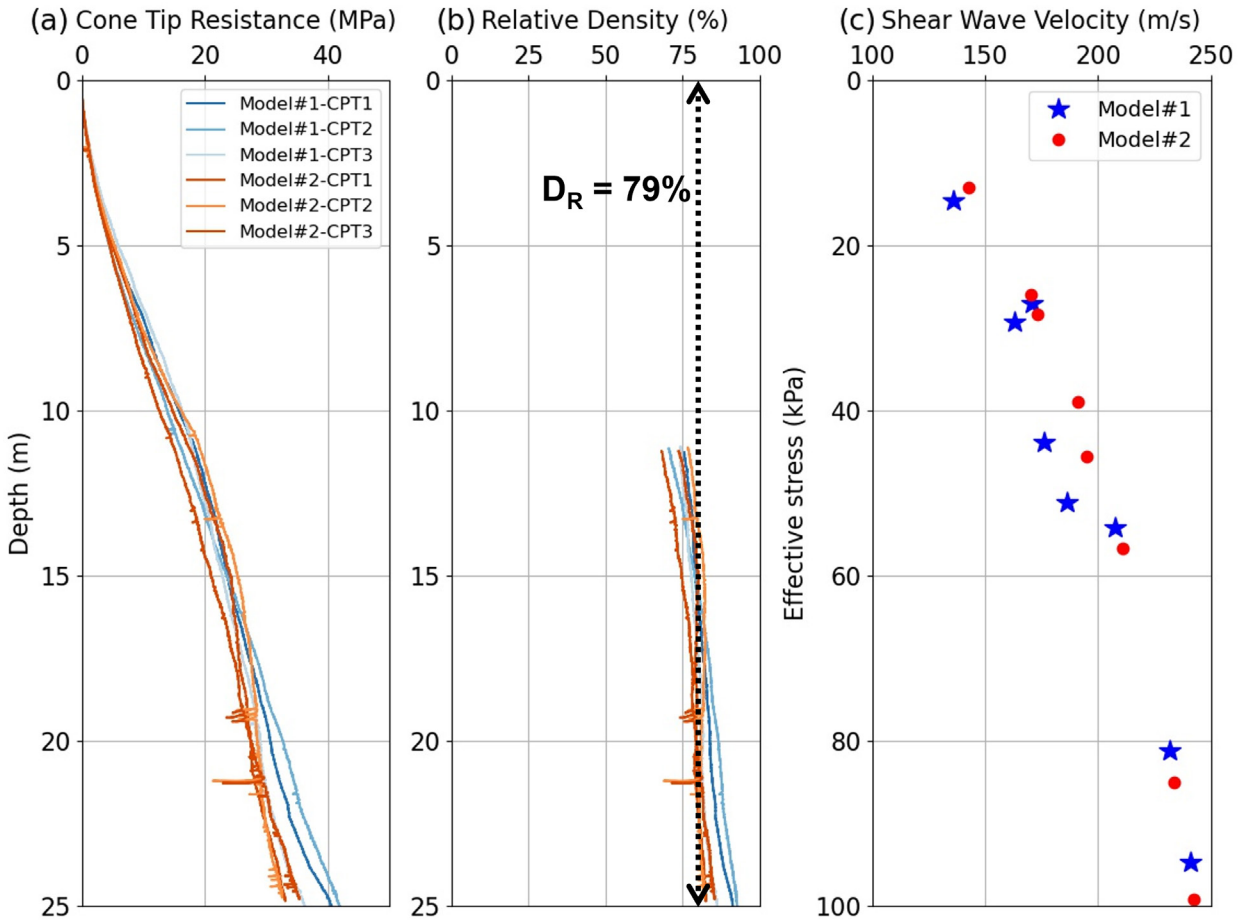

Figure 6. In-flight CPT and bender element results at various locations of the soil models

Monotonic Load Test Results

The test results indicate that the anchor tensile capacity increases as the load inclination angle decreases (*i.e.*, the angle becomes closer to horizontal) for both embedment depths. Also, for any given load inclination angle, the anchor capacity increases as the embedment is increased. The results of the load tests are presented in Figure 7a and 7b for the deeply and shallowly embedded anchors. For the deep tests performed at 30°, 45, and 70°, the tensile force increases with a steep slope during the initial 0.2 to 0.5 m of displacement. Subsequently, the load increased at a smaller rate during the remainder of the test. For the vertical load tests (*i.e.*, 90°), the load first reached a peak load at a small displacement, followed by a gradual decrease in force. The shallow tests mobilized their ultimate capacity in smaller displacements as compared to the deep tests. In addition, after reaching the peak load, all four shallow tests exhibited a rapid decrease in force, and the rate of post-peak force reduction increased as the load inclination angle decreased from vertical to horizontal.

The tensile capacity of the ring anchor increased by around 200% when the load inclination changed from vertical to 30° from horizontal for the shallow embedment case. In the deep embedment case, the increase in tensile capacity is even larger, reaching a magnitude of 300%. Figure 8 presents an interaction diagram illustrating the relationship between the ultimate tensile capacity of the ring anchors, load inclination angle, and embedment depth. This figure clearly shows the increase in capacity with increasing the anchor's embedment depth. Furthermore, the elongated shape of the interaction diagrams shows a significantly greater anchor capacity as the load is applied in a direction closer to the horizontal, highlighting the importance of considering the loading inclinations when designing ring anchors.

Discussion

Installation Disturbance Effects

Parallel to this centrifuge study, a series of Finite Element Modeling (FEM) analyses of monotonic load tests on ring anchors were calibrated against the centrifuge model results (Gogoi *et al.*, 2023). The FEM simulation utilized ABAQUS and CAE software with Mohr-Coulomb failure criteria adopted to simulate the ring anchor's behavior under tensile loading in dense sand conditions. The FEM simulations estimated a vertical tensile capacity for shallow and deep embedded conditions of 3.07MN and 13.69MN, respectively. The FEM overestimates the experimentally

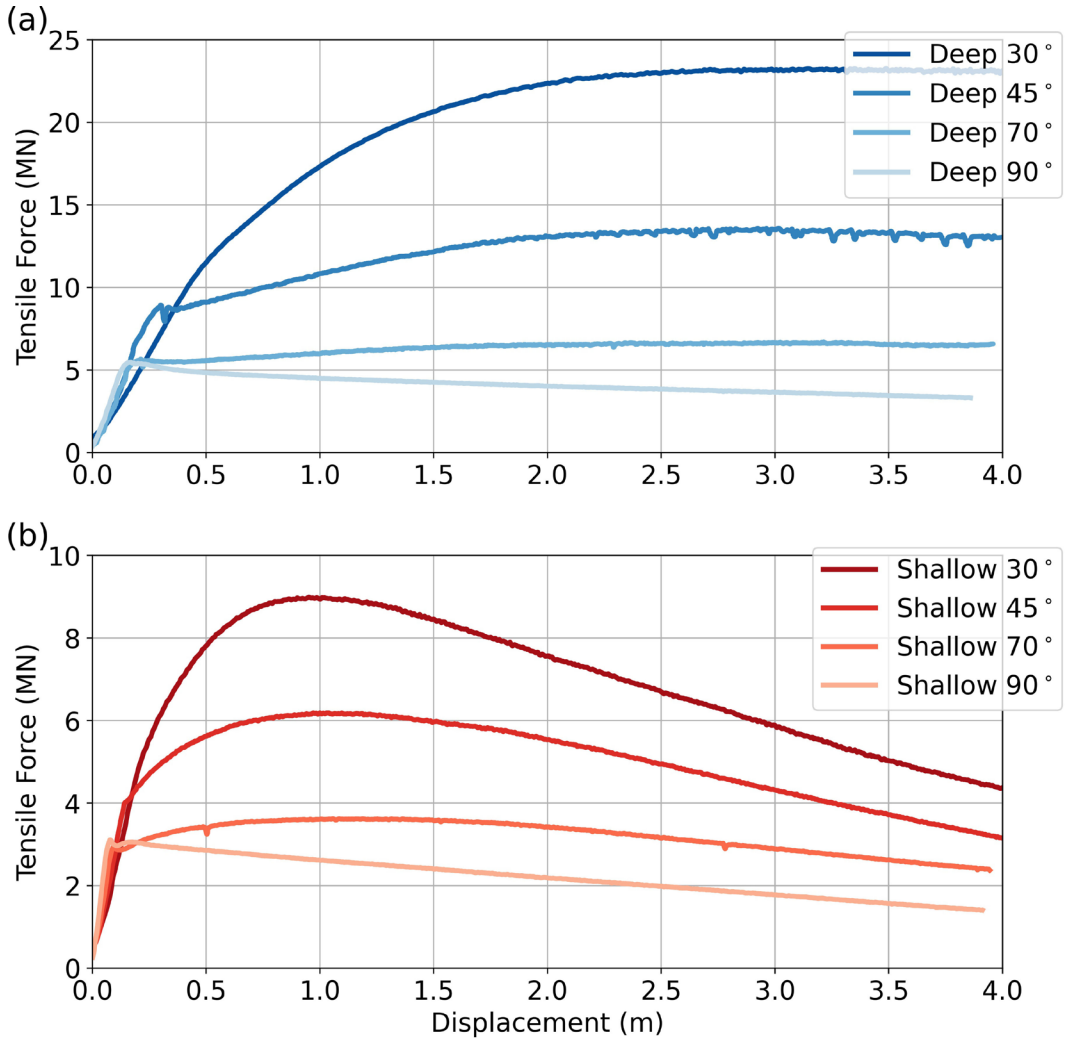

Figure 7. Results of monotonic tensile load test of ring anchor for both (a) deep and (b) shallow embedment cases (note the different y-axis ranges in the plots)

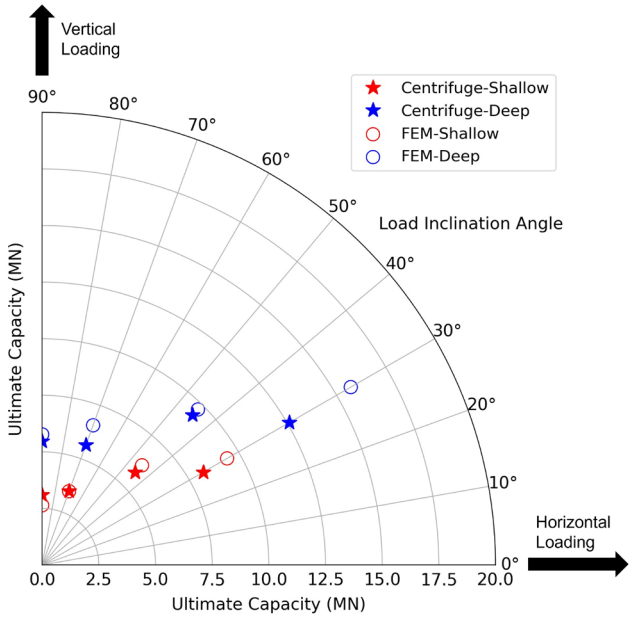

Figure 8. Ring anchor ultimate tensile capacity interaction diagram

measured capacity of 7.9MN for the vertical deep embedment case. One possible explanation for this discrepancy is the disturbance induced by the anchor installation process, which is not considered in numerical simulation. To investigate this, three CPT soundings were performed along the footprint of a deeply embedded 45-degree anchor installation. One CPT was conducted directly at the center of the pusher tube, while the other two were performed along the triangle wing with a spacing of 12 cm between them. Figure 9a shows the cone tip resistances with depth, while Figure 9b displays the computed relative density of the soil using the Mayne (2007) correlation. The star sign on each curve represents the depth reached by the anchor installation tool at each CPT location.

The CPT results revealed a significant decrease in the q_c and D_R of the soil at locations where the installation tool reached in comparison to the CPT sounding performed in an undisturbed location. The soil at the center of the installation tool exhibited the greatest level of loosening, resulting in a calculated relative density of less than 20%. This ob-

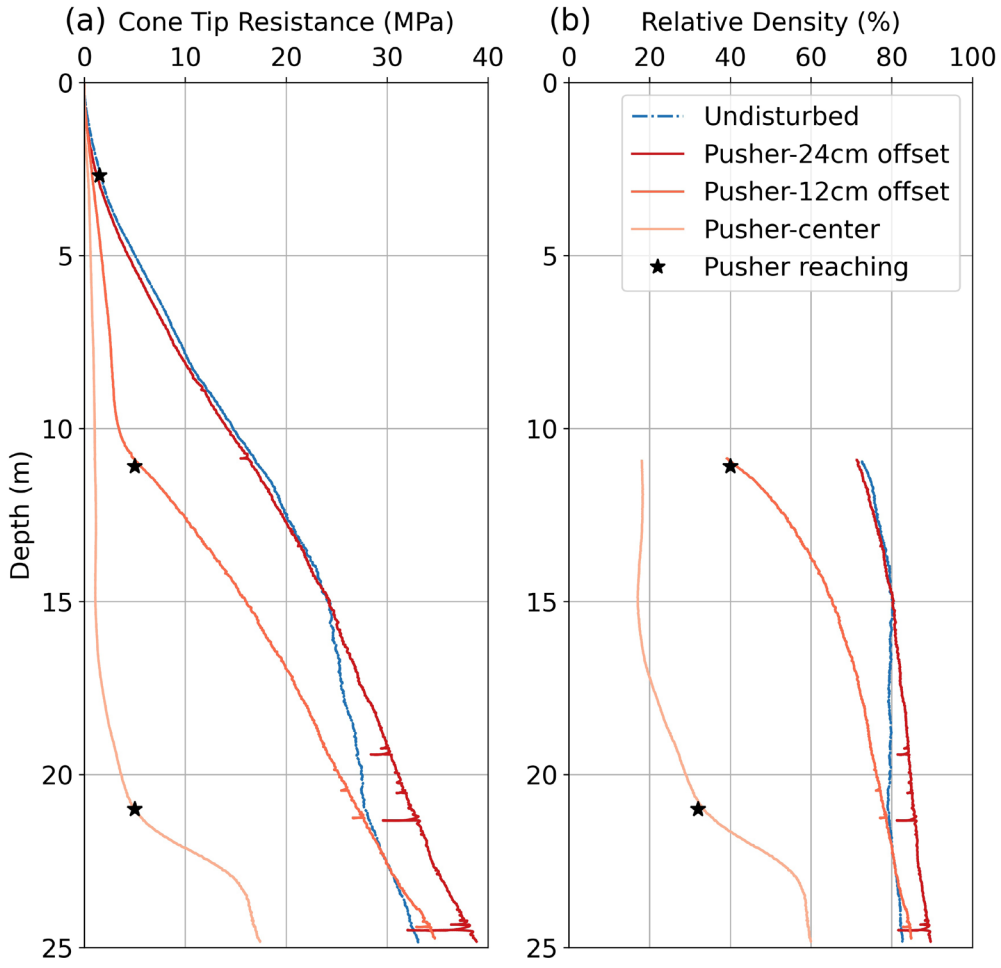

Figure 9. CPT result comparison between installation affect area and undisturbed zone

servation can be related to the anchor installation process, during which the anchor and pusher tube can be plugged with sand, displacing the sand radially outwards. When the pusher is detached from the anchor and removed from the soil, it can create a void where the sand caves into, leading to the continuous loosening of the soil column just above the anchor. Therefore, it is important to consider the installation effect when estimating the vertical capacity of ring anchors.

Anchor Failure Mechanism

The initial stiffness of the anchors was defined as the average slope of the load-displacement curve from the starting point to 50% of the peak tensile capacity. The initial stiffness for each case is plotted in Figure 10 as a function of the loading inclination angle. The figure shows that the initial stiffness of the anchor increases as the load inclination angle increases from 30° to vertical, with around 23MN/m at 30° inclination to around 35MN/m for vertical pulling irrespective of embedment depth.

This observation can be explained by the results of FEM simulation results presented in Gogoi *et al.* (2023). Figure 11 shows the contours of soil displacements for four

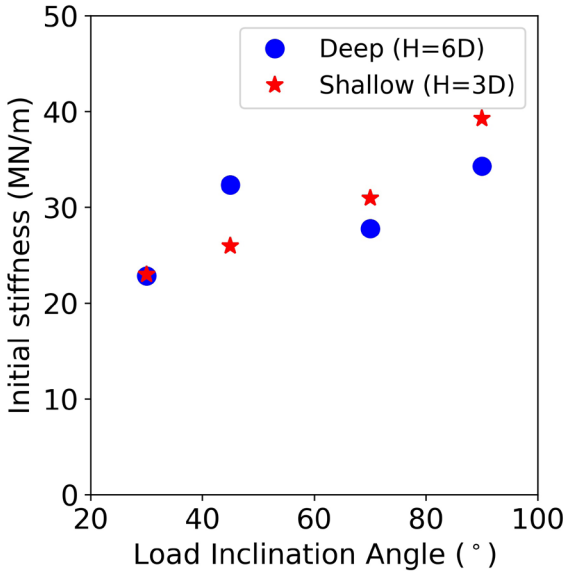

Figure 10. The initial stiffness of the anchor for various depths and load inclination angles

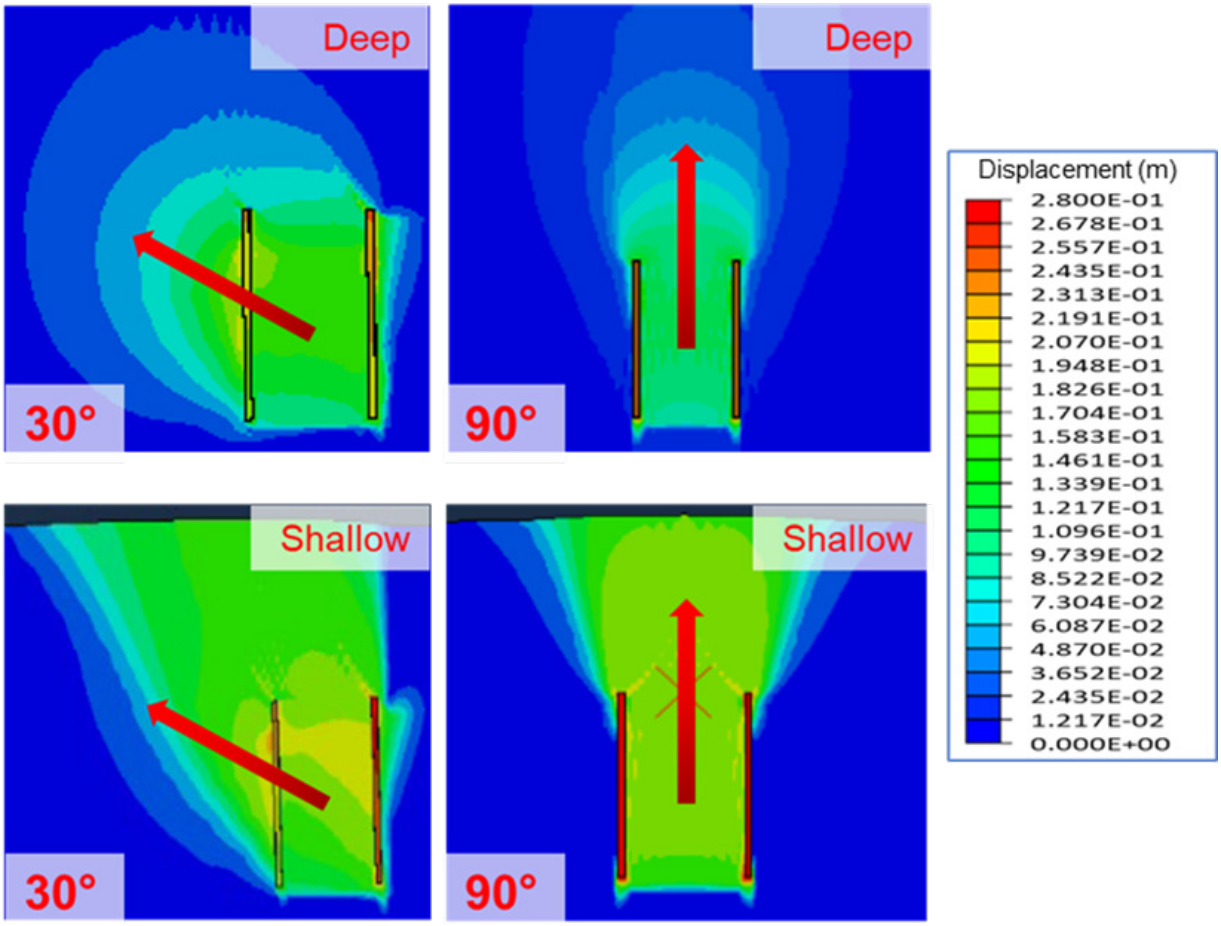

Figure 11. Displacement contours of the ring anchor under various loading conditions

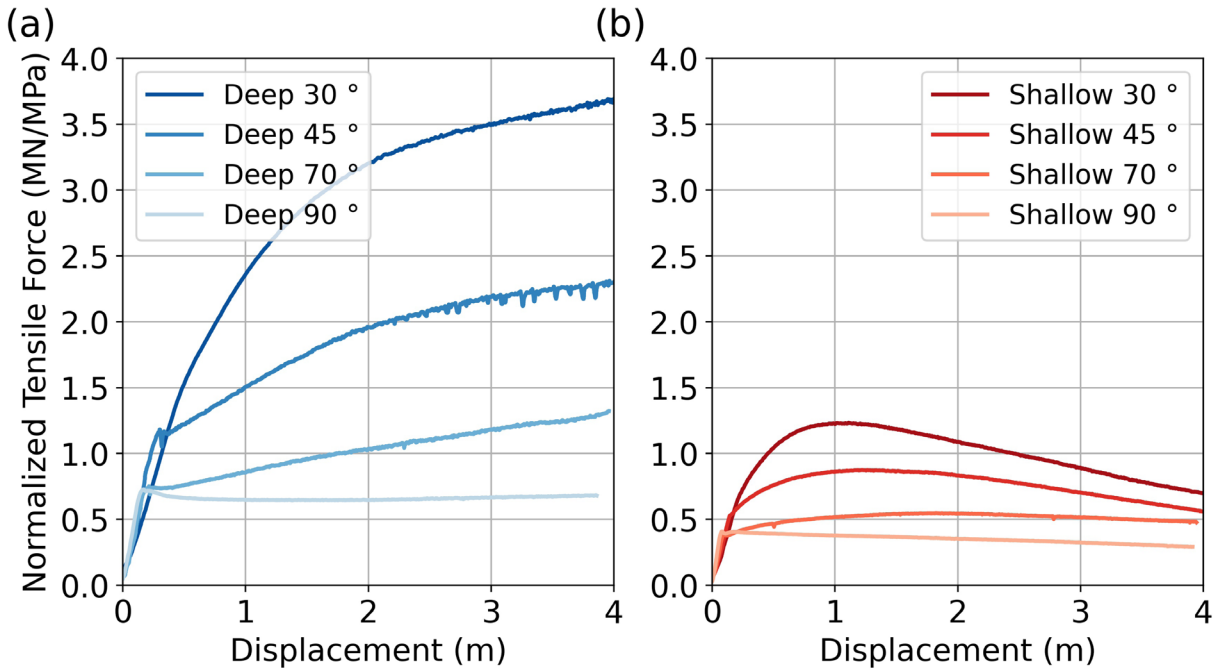

Figure 12. Results of monotonic tensile load test of ring anchor plotted with tensile force normalized by vertical effective stresses for (a) deep and (b) shallow embedment case

different scenarios. By comparing the displacement contours between the 30° and 90° scenarios, it is evident that the amount of mobilized soil increases as the load inclination angle changes from vertical to 30° in both shallow and deep conditions. Loading at 30° leads to the transfer of load in the form of passive resistances, leading to an initially softer soil-anchor interaction but mobilizing greater ultimate tensile capacities at sufficiently large anchor displacements (*i.e.*, Figures 7a and 7b).

The simulation result shows that when the embedment depth changes from deep to shallow, the ring anchor's failure mechanism changes from a flow-around deep failure mechanism to a cone-shaped failure mechanism where the failure plane reaches the surface of the soil. The failure mechanism change is evidenced by the continuously maintained post-peak force of the deep tests, in contrast to the decrease in force past the peak in the shallow tests, as shown in Figure 7a and 7b. Normalizing the tensile force data with the effective overburden stress can provide further evidence of this change in failure mechanism. Namely, the normalized force values are significantly greater for the deeply embedded anchors, as shown in Figure 12a and 12b. Such a sharp increase in capacity can be explained by a change in failure mechanism from the formation of a shallow wedge flow of soil to around the anchor in deeper locations, as further described in Wu *et al.* (2020).

Load-Displacement Coaxiality

The change in inclination angle of the wire rope was tracked during all tests to evaluate whether the anchor failure takes place preferentially in the horizontal or vertical directions. This data shows how much the wire rope deviates from the initial inclination, revealing how the anchor moves with respect to the direction of tensile loading. The wire rope inclination angle does not change if it moves in the direction of loading, the inclination angle increases if the anchor displaces in the horizontal direction more than in the vertical direction, and the inclination angle decreases if the anchor has a greater displacement in the vertical direction, as shown in Figure 13.

Figure 14a and 14b illustrate the inclination angle change with anchor displacement for the deep and shallow anchor tests, while Figure 14b and 14d show the inclination angle change with tensile loads. Data is not provided for the vertically loaded anchors because their inclination angle did not change during the tests. In both deep and shallow embedment cases, the load inclination angle initially increased until the peak tensile load was reached, indicating that the ring anchors experienced a greater horizontal displacement. Subsequently, the inclination angle gradually decreased, indicating a greater vertical anchor displacement. This trend is in agreement with the horizontal anchor capacity component being softer at small displacements but ultimately mobilizing greater capacities at large displacements. While the anchor displacements were not coaxial with the initial load direction, the changes in load inclination angle remained within a narrow range of –0.2° to +0.4°, suggesting only minor deviations.

Implications in Practice

The centrifuge tests presented in this paper characterize the load-displacement response of ring anchors embedded in sand and loaded monotonically. The results show that the embedded ring anchor is an efficient alternative to foundations that extend to the seabed surface. The capacity of the anchors greatly increased as the loading angle deviated from vertical due to two factors: (i) mobilization of lateral resistances and (ii) disturbance caused by installation. Regarding (i), the results highlight the benefit in configurations of mooring systems that result in loads that are closer to the horizontal. This creates a tradeoff, as this necessitates greater lateral spacings between adjacent wind turbines thus reducing the number that can be included in a project sites. Economic analyses can inform whether it is more cost-effective to have foundations that are likely larger in size and loaded at directions closer to the vertical or a smaller number of turbines. However, it is noted that the efficiency of energy generation also depends on the turbine spacing, which should also be taken into consideration. Future research efforts should be devoted to assessing whether similar installation disturbance effects as observed in the centrifuge tests are present in the field, especially considering that the ratio of anchor to particle size is significantly greater in the field. This could be addressed by post-installation CPT soundings, in a similar way as done in this centrifuge investigation, along with field anchor load tests. If similar disturbance effects are observed, then the designer may need to increase the anchor size if the loading direction is likely to be close to vertical or to implement ground improvement such as vibro-compaction.

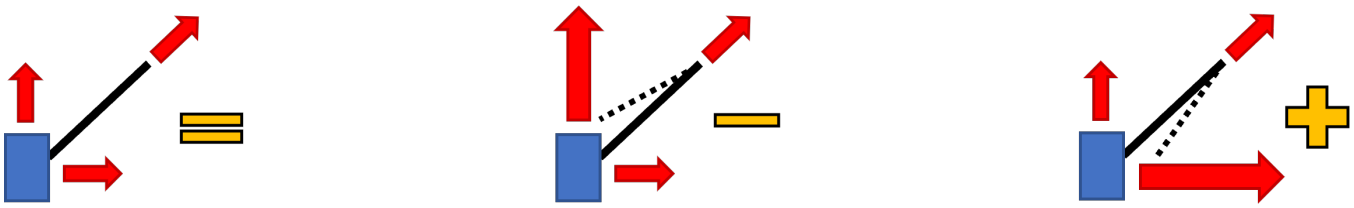

Figure 13. Relationship between anchor movement deviations and wire rope angle change. The initial line angle is shown by the solid line and the final line angle is shown by the dashed line

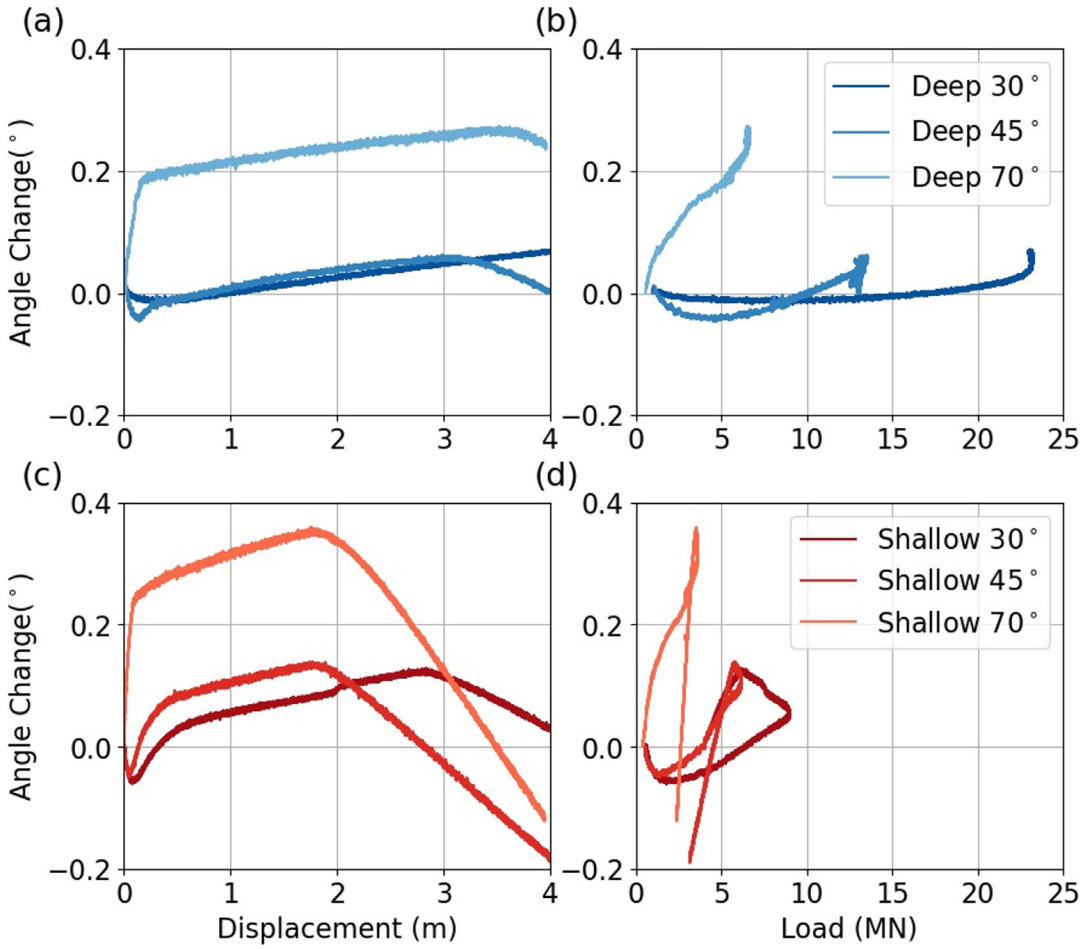

Figure 14. Wire rope angle changes plotted against anchor displacement (left) and load (right)

Conclusions

This paper presents the results of a centrifuge modeling investigation on the monotonic tensile loading behavior of ring anchors embedded in saturated sand. This study investigates the influence of anchor embedment depth and load inclination angle on the tensile capacity and load transfer behavior of the ring anchors. The key findings can be summarized as follows:

- Under monotonic tensile loading in sand, the tensile capacity of the ring anchor increases as the inclination angle decreases (*i.e.*, as the loading direction changes from vertical to horizontal). Specifically, when loaded at a 30° inclination from the horizontal, the anchor's tensile capacity is three to four times greater compared to when it is loaded vertically.
- The tensile capacity of the ring anchor also increases with greater embedment depth, attributed to a combined effect of the increase in overburden stress and changes in the failure mechanism. Specifically, the ratio between ring anchor tensile capacity in deep and shallow embedment cases are 2.6 and 1.8, for 30° and vertical inclination, respectively.
- Throughout the tensile loading process, the movement of the ring anchor is not perfectly coaxial with the direction of the applied tensile load, but the deviations are minor, limited within a range of ±0.4°. Initially, the anchors tend to move more in the horizontal direction, while after the peak load, they move more in the vertical direction.
- Multiple failure mechanisms are involved during loading of the anchors. The primary failure mechanism may vary depending on the depth, load inclination, and different stages of the test. Increasing the embedment depth leads to changes in the failure mechanism from a wedge that reaches the soil surface to one characterized by soil locally flowing around the anchor. Variations in load inclination changed the type of load transfer, with loading closer to the horizontal leading to greater passive resistances that in turn resulted in mobilization of a greater soil volume. These differences in failure mechanism are manifested in the differences in anchor initial stiffness.
- It is important to consider the effects of anchor installation when estimating the capacity of the ring anchors. In these experiments, anchor installation resulted in a calculated decrease of sand relative density

from 79% to 20%, mainly influencing the anchors' vertical capacity.

Acknowledgements

The authors would like to acknowledge the contributions of Ragini Gogoi, Junho Lee, Kyle O'Hara, Nathan Love, Tom Kohnke, Chad Justice, and Daniel Wilson. This material is based upon work supported by National Science Foundation under NSF Cooperative Agreement No. CMMI-1936939. The UC Davis Center for Geotechnical Modeling is supported under the grant CMMI-1520581. Any opinions, findings, conclusions, or recommendations expressed in this material are those of the author(s) and do not necessarily reflect those of the National Science Foundation.

References

Aubeny, C. (2017). *Geomechanics of marine anchors*. CRC Press.

Bastidas, A. M. P. (2016). Ottawa F-65 sand characterization (Doctoral Dissertation). University of California, Davis.

Beemer, R. D. (2016). Experimental studies of squat gravity caissons and monopiles for offshore applications (Doctoral dissertation).

Beemer, R. D., Biscontin, G., Murali, M., & Aubeny, C. P. (2018). Use of a MEMS accelerometer to measure orientation in a geotechnical centrifuge. *International Journal of Physical Modelling in Geotechnics*, 18(5), 253-265.

Bhattacharya, S. (2014). Challenges in design of foundations for offshore wind turbines. *Eng. Technol. Ref*, 1(1), 922.

Bureau of Ocean Energy Management. (2023). California Activities. Retrieved from https://www.boem.gov/renewable-energy/state-activities/california

Carter, J. M. F. (2007). North Hoyle offshore wind farm: design and build. *Proceedings of the Institution of Civil Engineers-Energy*, 160(1), 21-29.

Cha, M., Santamarina, J. C., Kim, H. S., & Cho, G. C. (2014). Small-strain stiffness, shear-wave velocity, and soil compressibility. *Journal of Geotechnical and Geoenvironmental Engineering*, 140(10), 06014011.

Diaz, B. D., Rasulo, M., Aubeny, C. P., Fontana, C. M., Arwade, S. R., DeGroot, D. J., & Landon, M. (2016). Multiline anchors for floating offshore wind towers. *OCEANS 2016 MTS/IEEE Monterey* (pp. 1-9). IEEE.

Fontana, C. (2019). A multiline anchor concept for floating offshore wind turbines (Doctoral Dissertation). University of Massachusetts, Amherst.

Gogoi, R., Aldawwas, A., Aubeny, C. P., Martinez, A., Huang, L., DeGroot, D., Arwade, S., & Beemer, R. (2023) Numerical analyses of a multiline ring anchor for floating offshore wind turbines in sand. *Proceedings of 10th European Conference on Numerical Methods in Geotechnical Engineering*. (Under Review)

Herduin, M. (2019). Multi-directional loading on shared anchors for offshore renewable energy: Definition and preliminary investigation into soil behavior and anchor performance (Doctoral Dissertation). The University of Western Australia.

Jardine, R.J., Overy, R.F., & Chow, F.C. (1998). Axial Capacity of Offshore Piles in Dense North Sea Sands. *Journal of Geotechnical and Geoenvironmental Engineering, Volume 124, Issue 2*.

Jensen, M.R., & Kellezi, L. (2023) Geotechnical characteristics of siliceous North Sea sands. *Canadian Geotechnical Journal, Volume 60, Number 10.*

Kim, J. H., Choo, Y. W., Kim, D. J., & Kim, D. S. (2016). Miniature cone tip resistance on sand in a centrifuge. *Journal of Geotechnical and Geoenvironmental Engineering* 142.3: 04015090.

Kutter, B. L. (1992). Dynamic centrifuge modeling of geotechnical structures. *Transportation research record*, (1336).

Lee, J., & Aubeny, C. P. (2019). Effect of wing plates on a multiline ring anchor system in cohesive soils. *OCEANS 2019 MTS/IEEE SEATTLE* (pp. 1-6). IEEE.

Lee, J., & Aubeny, C. P. (2020). Multiline Ring Anchor system for floating offshore wind turbines. *J. Phys.: Conf. Ser*. 1452 012036

Lee, J., Khan, M., Bello, L., & Aubeny, C. P. (2020). Cost Analysis of Multiline Ring Anchor System for Offshore Wind Farm. *45th Annual Conf. on Deep Foundations*, 2020

Lopez, A., Green, R., Williams, T., Lantz, E., Buster, G., & Roberts, B. (2022). *Offshore Wind Energy Technical Potential for the Contiguous United States* (No. NREL/PR-6A20-83650). National Renewable Energy Lab. (NREL), Golden, CO (United States).

Martinez, A., Palumbo, S., & Todd, B. D. (2019). Bioinspiration for anisotropic load transfer at soil–structure interfaces. *Journal of Geotechnical and Geoenvironmental Engineering*, 145(10), 04019074.

Mayne, P. *Cone penetration testing*. Vol. 368. Transportation Research Board, 2007.

Musial, W., Beiter, P., Spitsen, P., Nunemaker, J., & Gevorgian, V. (2019). *2018 Offshore Wind Technologies Market Report.* U.S. Department of Energy (DOE), doi:10.2172/1572771.

Wu, J., Kouretzis, G., Suwal, L., Ansari, Y., & Sloan, S. W. (2020). Shallow and deep failure mechanisms during uplift and lateral dragging of buried pipes in sand. *Canadian Geotechnical Journal*, 57(10), 1472-1483.

Zhao, L., Bransby, M. F., & Gaudin, C. (2020). Centrifuge observations on multidirectional loading of a suction caisson in dense sand. *Acta Geotechnica*, 15, 1439-1451.

DFI Journal Underwriters